BRL

MEMORANDUM REPORT NO. 1871

ATMOSPHERIC EFFECTS ON THE BEAM PROPAGATION OF THE XM-23 LASER RANGEFINDER

by

Paul H. Deltz

September 1967

U. S. ARMY MATERIEL COMMAND
BALLISTIC RESEARCH LABORATORIES
ABERDEEN PROVING GROUND, MARYLAND

B A L L I S T I C R E S E A R C H L A B O R A T O R I E S

MEMORANDUM REPORT NO. 1871

SEPTEMBER 1967

ATMOSPHERIC EFFECTS ON THE BEAM PROPAGATION OF THE XM-23 LASER RANGEFINDER

Paul H. Deitz

Ballistic Measurements Laboratory

Presented at the "Laser Range Instrumentation Seminar-in-Depth" sponsored by the Society of Photographic Instrumentation Engineers held in El Paso, Texas, 16-17 October 1967.

RDT&E Project No. 1W523801A291

A B E R D E E N P R O V I N G G R O U N D, M A R Y L A N D

B A L L I S T I C R E S E A R C H L A B O R A T O R I E S

MEMORANDUM REPORT NO. 1871

PHDeitz/cr
Aberdeen Proving Ground, Md.
September 1967

ATMOSPHERIC EFFECTS ON THE BEAM PROPAGATION OF THE XM-23 LASER RANGEFINDER

ABSTRACT

A special optical receiver with a 2-foot input aperture was used to measure beam cross sections of the XM-23 Laser Rangefinder. The standard deviations of the received energies were determined for path-lengths from 200 to 1500 meters. The index structure constant, C_n, (derived from the measured thermal structure function) and the solution to the spherical wave equation were used to predict the standard deviations of the optical energy distributions. The predictions based on meteorological measurements were compared to the standard deviations of the optical measurements for high scintillation conditions.

TABLE OF CONTENTS

LIST OF ILLUSTRATIONS

INTRODUCTION

Recently the Ballistic Research Laboratories (BRL) conducted a study to determine the distribution of energy in the beam of the newly developed XM-23 Laser Rangefinder. This study is part of a comprehensive program to determine the potential eye hazard to friendly troops when the laser rangefinder is used in tactical situations.

The distribution of energy in the beam was determined from measurements of the densities of photographic images of the laser beam. The beam was intercepted by an optical system with a 24-inch parabolic mirror as its principal element. The beam reflected from the mirror and light from a calibrated step wedge were transmitted to the film plane of the system. A densitometer was used to measure film densities which were then converted to relative energies.

Data derived from one-dimensional (i.e., uni-directional) scans of the film records were plotted and used to establish distribution probability curves which show the frequency of occurrence of normalized energies in the beam.

Cross section measurements of the beam were made for each of the three cavities used with the XM-23 rangefinder; for each cavity, measurements were made over four pathlengths --- 200, 600, 1000 and 1500 meters. Standard deviations of the optical data were computed from the cumulative distribution curves of the energies.

Direct meteorological measurements of an index structure constant, C_n, were made also. This constant relates directly to the magnitude of the refractive index fluctuations in the turbulent medium and hence to the optical variance. Comparisons were made between the measured C_n's and C_n's derived from the optical data.

THEORY

After an electromagnetic wave travels 100 meters or more through the atmosphere, the cross section of the wave begins to exhibit marked changes. These changes are caused by diffractive interaction of the wave with a medium having a varying index of refraction. The effects of intensity modulation along the path are multiplicative rather than additive; thus, the log-intensity, rather than the intensity, is modulated in an additive fashion. The variations of the log-normalized intensities should follow a normal distribution as a consequence of the central-limit theorem.

An important factor in the evaluation of the propagation characteristics of an electromagnetic wave is the nature of the three-dimensional medium. The statistics of the mixing of air pockets at various temperature are given by the Kolmogoroff theory[1] which presumes that the medium receives energy represented by low wave number turbulence at wavelengths much longer than those which affect atmospheric transmission. No energy is dissipated in heating effects; the energy cascades down through higher and higher wave number turbulence until the smallest cell size, known as the inner scale, is reached. Only cell sizes between the outer scale, L_o (on the order of the beam height above the ground), and the inner scale, l_o (a few millimeters), affect propagation.

As a consequence of the Kolmogoroff theory, a structure function can be written giving the mean squared difference of the index of refraction, measured at two points separated by a distance, r, as $C_n^2 r^{2/3}$. The line connecting the two points is horizontal and perpendicular to the direction of wind flow. The index structure constant can also be related to the vertical temperature gradient. Due to the nature of

---

[1] Kolmogoroff, Turbulence, Classic Papers on Statistical Theory, S. K. Friedlanders and L. Topper, Eds., Interscience Publishers, John Wiley & Sons Inc., New York, 1961, page 151.

turbulent mixing, the preferential direction of the initial turbulence generation is assumed to have been lost so that the spectral densities of the index wave numbers above the outer scale are independent of direction. Hence the medium is isotropic in the region of influence to optical propagation.

Using these and other assumptions, Tatarski[2] has predicted the variance of intensities at a point in a plane perpendicular to the direction of propagation as

$$\sigma^2 = 1.23\, C_n^2\, k^{7/6} L^{11/6} \qquad (1)$$

where σ is the standard deviation of the log-normal distribution of a plane wave, C_n is the index structure constant, k is the wave number of the light $(2\pi/\lambda)$, where λ is the wavelength, and L is the pathlength. The solution for the variance of intensities in a spherical wave is identical to Equation (1) except for a constant which is a factor of approximately 2.4 lower.[3]

MEASUREMENT APPROACH

Nearly all previous propagation experiments have been conducted with continuous wave sources. Tatarski's theory calls for the wind direction angle relative to the optical path to be much larger than the quantity $(\lambda/L)^{1/2}$. In the typical experiment, as the three-dimensional cell structure floats across the optical path, the normal wind component, v_n, provides scanning while the intensity is monitored at an aperture as a function of time. Statistical operations then yield the distribution functions.[4]

---

[2] Tatarski, Wave Propagation in a Turbulent Medium, Vol. I, McGraw-Hill, 1961, page 211.

[3] Ibid. See Equation 9.43. $\overline{\chi^2}$, the variance of the log-amplitude, is one-fourth of σ^2, the variance of the log-intensity.

[4] Ibid. See Chapter 12. Also D. L. Fried, *et al.*, J. Opt. Soc. Am. 57, 787 (1967).

The temporal fluctuations of intensity are related to the spatial fluctuations by

$$T = S \cdot v_n \qquad (2)$$

where T is measured in hertz, S in cycles per meter, and v_n in meters per second. The statistical character of the space domain, often of principal interest, is inferred through S and v_n, although many problems are encountered through necessary assumptions relating to medium isotropy, homogeneity along the optical path, beam divergence, and the time constant of the cell structure of the medium.

The approach used by ERL in recent tests with a helium-neon laser, involves a measurement in the space domain by photo-optical methods.[5] This general method is the only one suitable for measuring the cross sections of pulsed laser beams.

Figure 1, a ray tracing, shows the path of rays incident on the optical receiver. Collimated light falling on an f/5 parabolic mirror is reflected off-axis to an optical flat and then from the flat to a focal point. An aperture placed at the focal plane restricts the field of view of the receiver to about 0.2 degree. A 6-inch focal-length lens placed one focal length from the aperture collimates the light passing through the aperture. The collimated light passes through an interference filter at the wavelength of the laser. Thus, a high signal-to-noise ratio is achieved by both the restriction of the field of view and the narrow bandpass filtering.

The image representing the two-dimensional spatial intensity distribution of the radiation at the plane of the parabolic mirror appears just beyond the interference filter. At this first image plane, a calibrated step wedge is projected so that the image of a set of known intensities is transmitted by a second lens to the film place where it appears along with the image representing the intensity distribution at the parabolic mirror.

---

[5] P. H. Deitz, "Optical Method for Analysis of Atmospheric Effects on Laser Beams," Proceedings of the Symposium on Modern Optics, Vol. XVII, Brooklyn Polytechnic Press, Fall 1967 (in press).

MEASUREMENTS AND ANALYSIS

Three cavities were supplied with the XM-23 rangefinder. The energy outputs of the three are nearly the same, about one-tenth of a joule delivered in a 30-nanosecond pulse. The laser wavelength is 6943 Å; the axis of polarization is horizontal for cavities Numbers 4 and 14, and vertical for Number 7.

Twenth-one runs were made at pathlengths ranging from 200 to 1500 meters with each combination of pathlength and cavity being used at least once. The path height averaged about 2 meters over medium grass. Kodak Tri-X film was used in all the runs. The response of this film, though considerably lower at the laser wavelength, was adequate for the energy available. Neutral density filters were used to attenuate the beam directly in front of the first lens. The densitometer which provided the calibrated step wedge was filtered at 6943 Å, the laser wavelength. During the normal data runs the step wedges were photographed before and after the laser shots.

We analyzed the film by using a densitometer to scan first the image of a step wedge and then the beam image. The scan across the beam image followed two vertical paths through fiducial marks on the film. Two vertical scans were made of each image because of the symmetry of the beam cross section. The output of the densitometer was in an analogue format and was recorded on magnetic tape, digitized, and processed by an electronic computer. The transmissions of the step wedge were converted to densities and plotted against the relative energies of the calibrated step wedge to form a characteristic curve. The characteristic curve along with two sets of energy scans, distribution curves, and cumulative distribution curves were automatically plotted for each photograph.

An analysis has been made of the potential sources and magnitudes of errors in the measurement procedure from the optical recording to the data reduction processes. Such factors as geometrical distortion, intensity modulation due to vignetting, and sensitometric step-wedge

calibration in the optical receiver, as well as film reduction characteristics, including reciprocity failure, dynamic range, and densitometer transfer function, have been considered and measured. Of the possible experimental errors, the densitometer response and reciprocity failure are considered the two major ones. The densitometer transfer function falls off gradually to about 50 percent at the effective limit of resolution of the system set by the scanning aperture (on the order of 40 microns, equivalent to just over 1 millimeter in object space). Reciprocity failure is the least understood phenomenon. A preliminary test indicated a slightly lower slope for the characteristic curve when exposed in 30 nanoseconds than when the exposure was of 1/2-second duration. However, this effect is offset by the characteristics of the data and the analysis method which follows.

RESULTS AND COMPARISON WITH THEORY

Figure 2 shows the cross section of the XM-23 rangefinder beam at 200 meters. The step wedge appears at the left of the image.

Figure 3 shows the cross section of the beam at 1500 meters, while Figure 4 shows the characteristic curve for the step wedge photographed during this run. Figures 5 to 10 show relative energy versus distance, percent occurrence of normalized energy and the summed percent of log of normalized energy for each of the two scans made through the image of the beam. Figures 11 through 18 show the photographs of the beam curves for a run made at 1000 meters.

The energy scan shown in Figure 5 is typical of the cross-sectional pattern of a light beam after propagation through a turbulent medium. The average energy for this scan was 0.08 relative units. Comparing the points in the scan with this average value, one observes many points close to, but below, this average. Fewer high points appear in the scan but some of those that occur extend to a factor of five above the average. This is a characteristic of a log-normal distribution and can be seen more clearly in Figure 6.

The energies from the scan represented by Figure 5 were normalized by dividing the average energy, and a histogram of occurrences was formed by counting the number of occurrences between E and E + ΔE, adjusted so that the area under the curve equals unity. The mode does not occur at the mean energy but at about 0.3 the average beam energy. There are higher excursions, however, to more than 4.5 times the average energy, but they occur much less frequently.

The effects of reciprocity failure and the densitometer transfer function tend to act as low bandpass filters on the optical signal. These factors have the least effect on data in the lower dynamic ranges of the film but tend to clip the peaks of the energy curves. When a log-normal distribution is integrated, and the summed percentage number of occurrences is plotted on a probability axis against the log of the normalized energies, a straight line results. If the log-normal distribution of optical energies holds, the cumulative distribution curve slope through the first two-thirds of integration (where the majority of readings occur) can be used to extrapolate to the final portions of the curve where bandpass filtering would evidence itself and the statistics, themselves, would not be as good. Figure 7 shows the integral curve. At the level of the average beam energy (zero on the log axis), over 70 percent of the occurrences have taken place. If a straight line is fitted to this plot, the difference between the 84 percent and 50 percent levels can be used to compute the standard deviation of the normalized energies.

An effort was also made to derive C_n through temperature lapse measurements at five stations along the beam path. However, these data were not used because, after statistical processing, the computed temperature differences were not sufficiently accurate to give meaningful results.

Equation (1) was solved for σ. The pathlength and measured C_n were then used to compute a predicted σ to compare with the measured optical σ. Table I shows a compilation of the parameters and results for each run. The measured values of σ for each of the two optical scans for 20 of the 21 runs are listed along with the measured values of C_n.

One of the objectives of the experiment was to give an analysis of the "worst possible case" to be expected in the propagation of the rangefinder beam. If the theory is indeed valid and the energies are log-normally distributed, then a "worst case" C_n can be used to extrapolate the cumulative distribution curves to the expected worst case for each pathlength. This approach can only be valid, however, for optical configurations which approximate a plane or spherical wave, i.e., a wave that in the absence of the atmosphere would give a uniform distribution of energies across a scan. It was realized that this condition would be present only at the longer pathlengths where a small part of one of the lobes shown in Figure 2 would be covering the parabolic mirror.

The computer program was written to eliminate sections of the energy scans at the fog background of the film from each end of the scan, but the beam profile indicated in the scans from the 200 meter and some of the longer pathlength photographs weighted the distribution curves toward the low-energy end of the abscissa. The asterisks in the measured optical σ column indicate those scans which yielded cumulative distribution curves exhibiting good fit to true log-normality. The scans associated with each of these cumulative curves show a marked absence of beam profile bias. This factor would suggest that some of the other distribution curves might be made to conform better to log-normal distributions by adjusting the energy scans with the unperturbed beam profile curve and by recomputing the distributions.

To date, few, if any, measurements with either CW or pulsed light sources have been made of all the variables indicated in Equation (1). Hence the constant of the equation has been only roughly verified. To test the validity of this relationship, the constant C_n, the pathlength,

and the plane wave coefficient were used to compute a predicted σ. A difference ratio was formed of the measured optical σ to the σ predicted through C_n. Nearly all of the predicted standard deviations were higher than the measured values up to an order of magnitude. Then the coefficient 1.23 was reduced by a factor of 2.36 to the coefficient given for the spherical wave solution. It is the spherical wave coefficient, along with the appropriate variables, that was used to compute the predicted standard deviation in Table I. The next column gives the difference ratios for the two scans. Generally the short path runs show a greater standard deviation and the long path runs a smaller standard deviation than predicted. As mentioned earlier, however, only the longer path runs achieved a reasonable experimental approximation to the theoretical model.

CONCLUSIONS

Even if the theoretical optical parameters were fully met, it would be useless to try to make a rigorous comparison between the measured variances and the predicted variances through C_n because of the extreme complexity of determining the true statistical character of the medium. C_n is not a constant along the optical path as can be seen from the temporal fluctuations of C_n at one station. In addition, all of the measurements were made during the mid-afternoon so that high scintillation conditions would persist. The theory describes light propagation under near neutral conditions; so buoyancy effects are not present and the medium is isotropic. High scintillation conditions are accompanied by high lapse conditions, and the limit to which the theory adequately describes the characteristics of light propagation for these conditions is not well known.

Table I

Run	Date	Cavity	Range	Frame	σ Meas.**** 1st Scan	σ Meas.**** 2nd Scan	C_n**	Pred.σ	Diff. Ratio*** 1st Scan	Diff. Ratio*** 2nd Scan
1	10 May 67	7	200	11	--	--	--	--	--	--
2	10 May 67	7	600	12	.26	.30	--	--	--	--
3	10 May 67	7	1000	16	.34*	.23*	--	--	--	--
4	10 May 67	7	1500	22	.25	.33	--	--	--	--
5	12 May 67	7	200	11	.34	.29	4.60	.210	1.57	1.33
6	12 May 67	7	600	13	.45	.57	4.32	.536	.84	1.10
7	12 May 67	7	1000	21	.32	.54	4.10	.816	.39	.66
8	12 May 67	7	1500	22	.28	.19	4.10	1.170	.24	.16
9	10 May 67	14	200	16	.31	.26	1.46	.067	4.63	3.98
10	10 May 67	14	600	14	.34*	.29*	1.02	.126	2.70	2.30
11	9 May 67	14	1000	15	.29*	.52	2.93	.583	.50	.90
12	9 May 67	14	1500	25	.24*	.28*	3.82	1.090	.22	.26
13	25 May 67	4	200	10	.25	.33	--	--	--	--
14	25 May 67	4	600	7	.48*	.35	3.58	.444	1.08	.80
15	25 May 67	4	1000	12	.43*	.41*	4.10	.816	.53	.50
16	25 May 67	4	1500	8	.33*	.39*	3.81	1.090	.30	.36
17	26 May 67	4	1500	8	.33*	.32*	3.30	.940	.35	.34
18	6 Jun 67	4	1000	15	.50*	.53	2.55	.507	.99	1.05
19	6 Jun 67	4	1500	8	.43*	.52*	3.81	1.090	.39	.48
20	6 Jun 67	14	1000	15	.34*	.34*	6.13	1.220	.28	.28
21	7 Jun 67	14	1500	13	.29*	.42*	3.16	.900	.32	.47

*Cumulative distribution curves show good fit to true log-normality

**$x\ 10^{-7} m^{-1/3}$

***Difference ratio = $\frac{\sigma \text{ meas}}{\sigma \text{ pred}}$

****Common log standard deviations

However, the optical data are significant as representative measurements of actual variances of the received energies in a practical situation. And the values of C_n give an indication of the scintillation conditions under which the measurements were made.*

ACKNOWLEDGEMENT

The author would like to express his appreciation to Mr. George J. Stiles for the C_n measurements and to Mr. James Lindenmuth and Miss Roberta Craig for the film scanning and computer data reduction.

*As a rough estimate, C_n can be taken to be on the order of $2 \times 10^{-6} m^{-1/3}$ for the "worst case" condition. Measured values of C_n appear to be higher than given in some of the literature, although the proximity to the ground might account for this. See J. Davis, Applied Optics, Vol. 5, No. 1, page 141, January 1966.

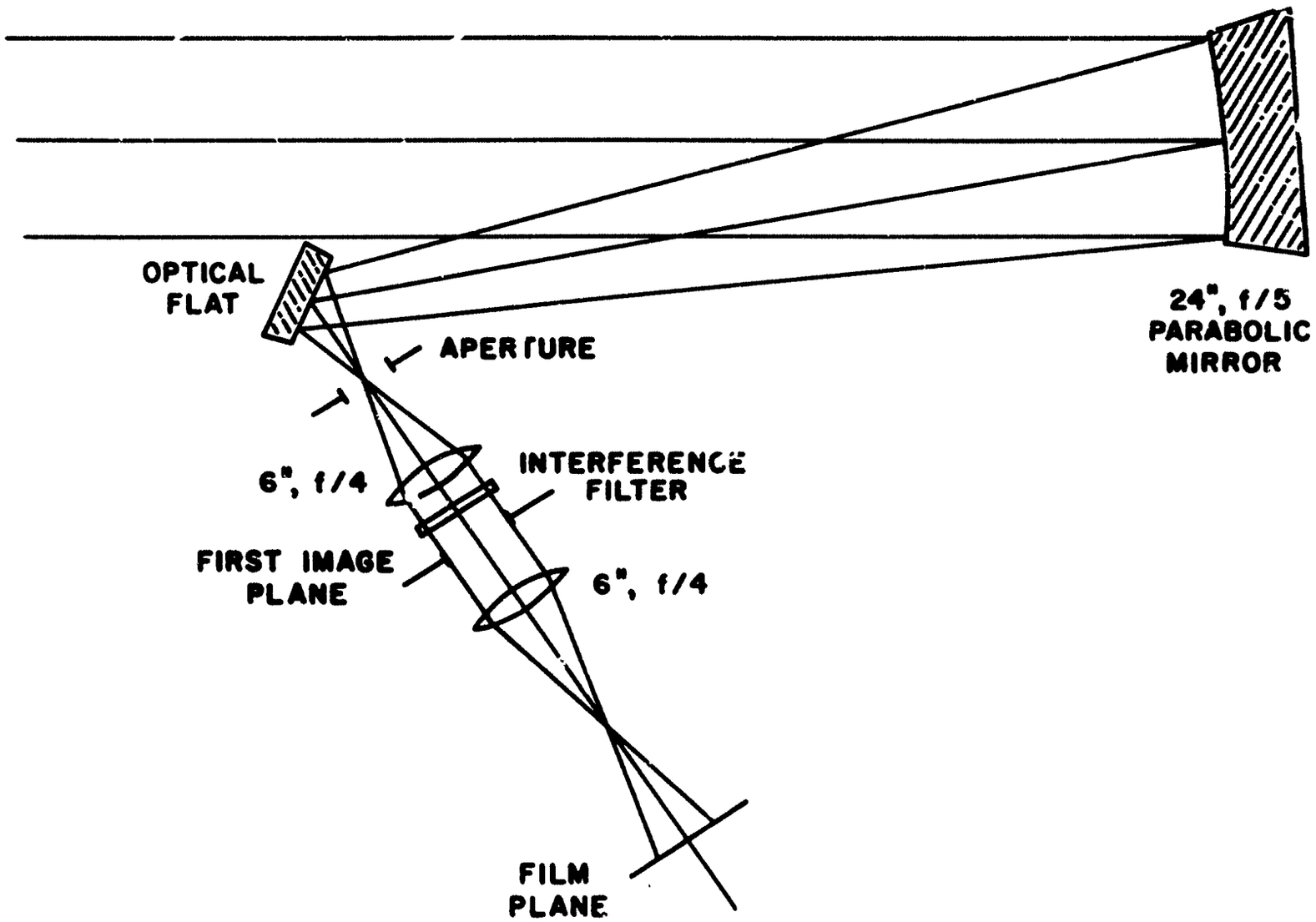

Figure 1. Ray diagram of optical receiver

Figure 2. Cross section of laser beam at 200 meters, calibrated step wedge is also shown

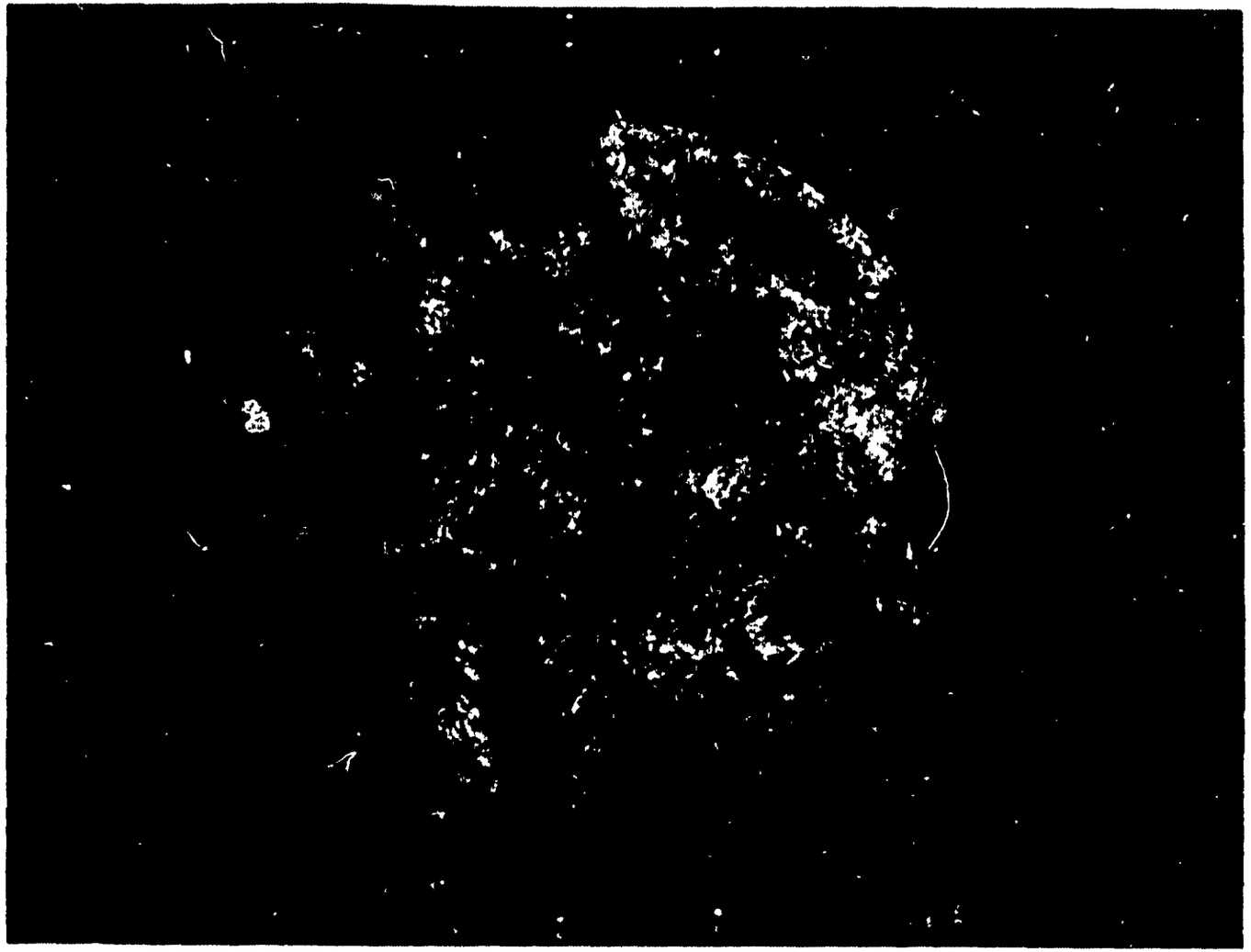

Figure 3. Cross section of laser beam at 1500 meters (Run No. 17)

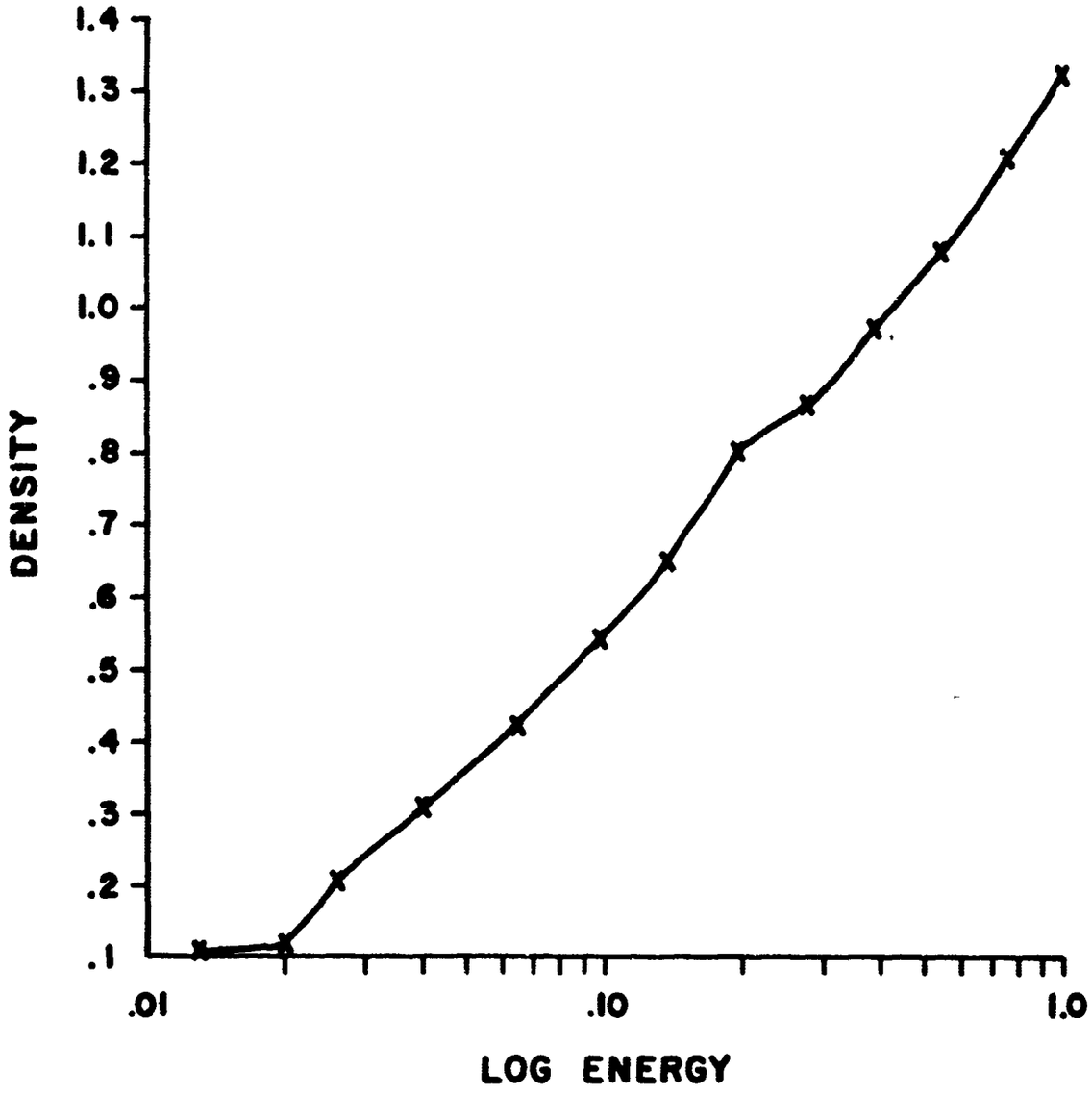

Figure 4. Characteristic curve for step wedge (Run No. 17)

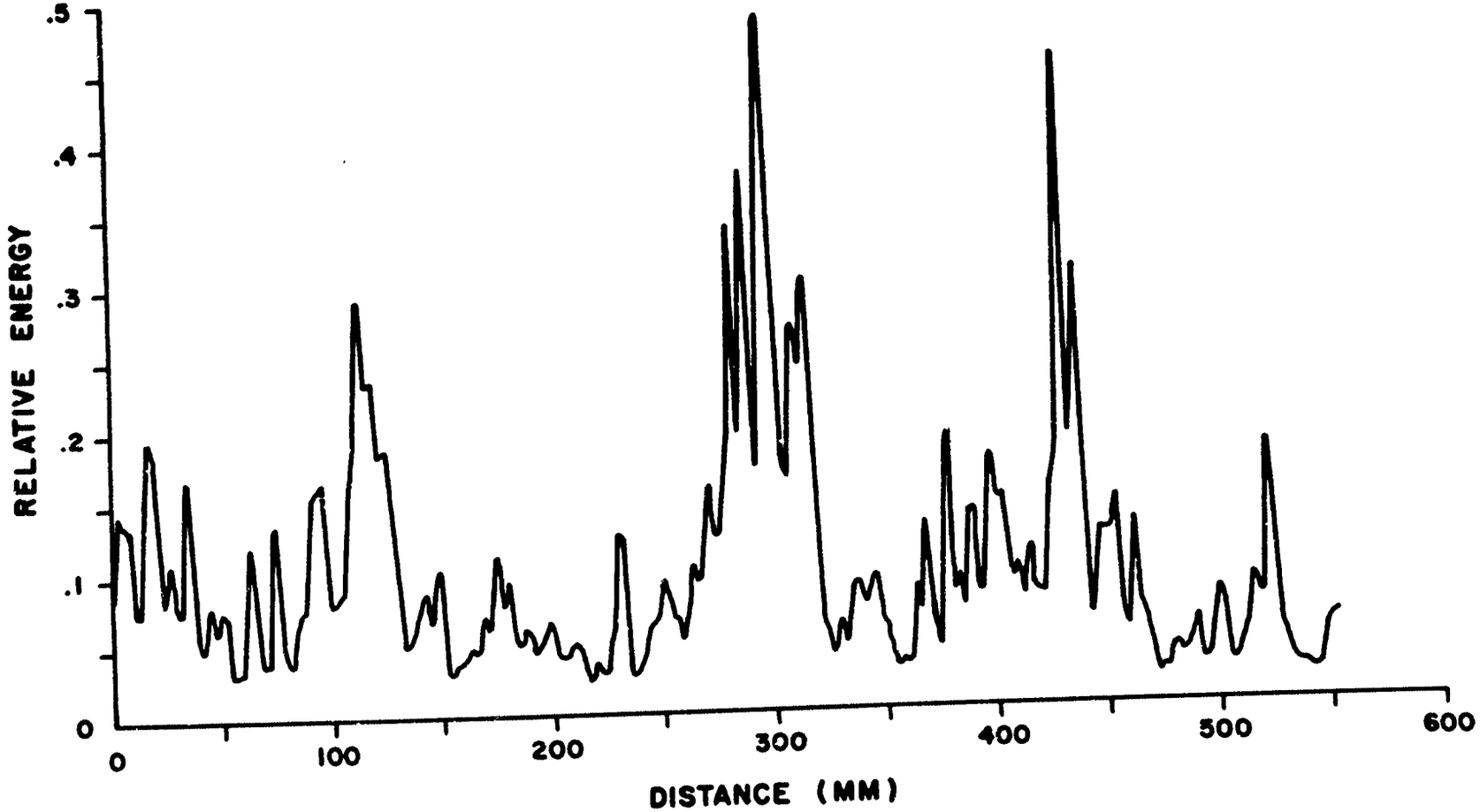

26 MAY 67, C 4, R 1500, FR 8 .

Figure 5. First energy scan for image shown in Figure 3

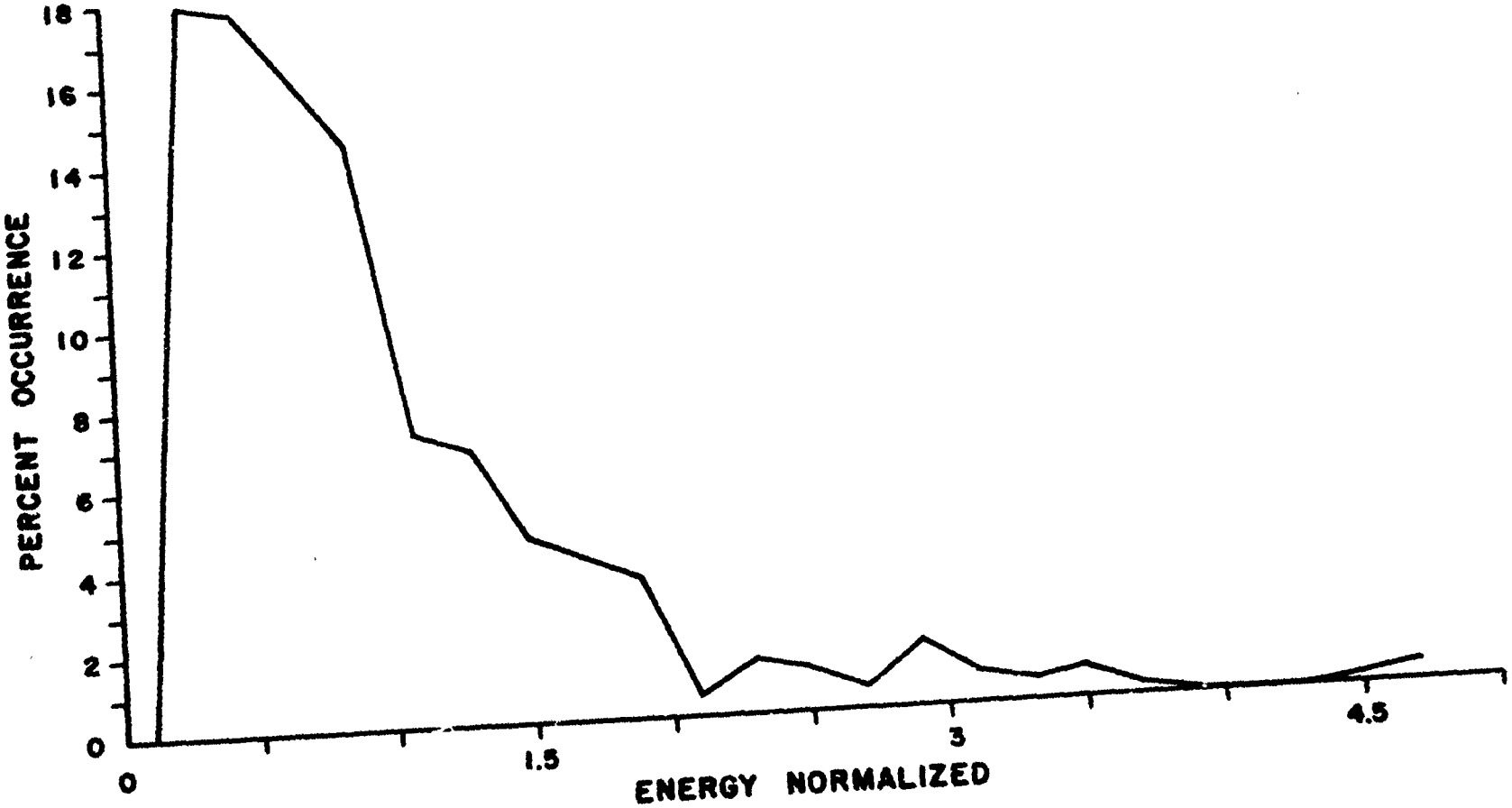

26 MAY 67, C 4, R 1500, FR 8 .

Figure 6. First distribution curve for image shown in Figure 3

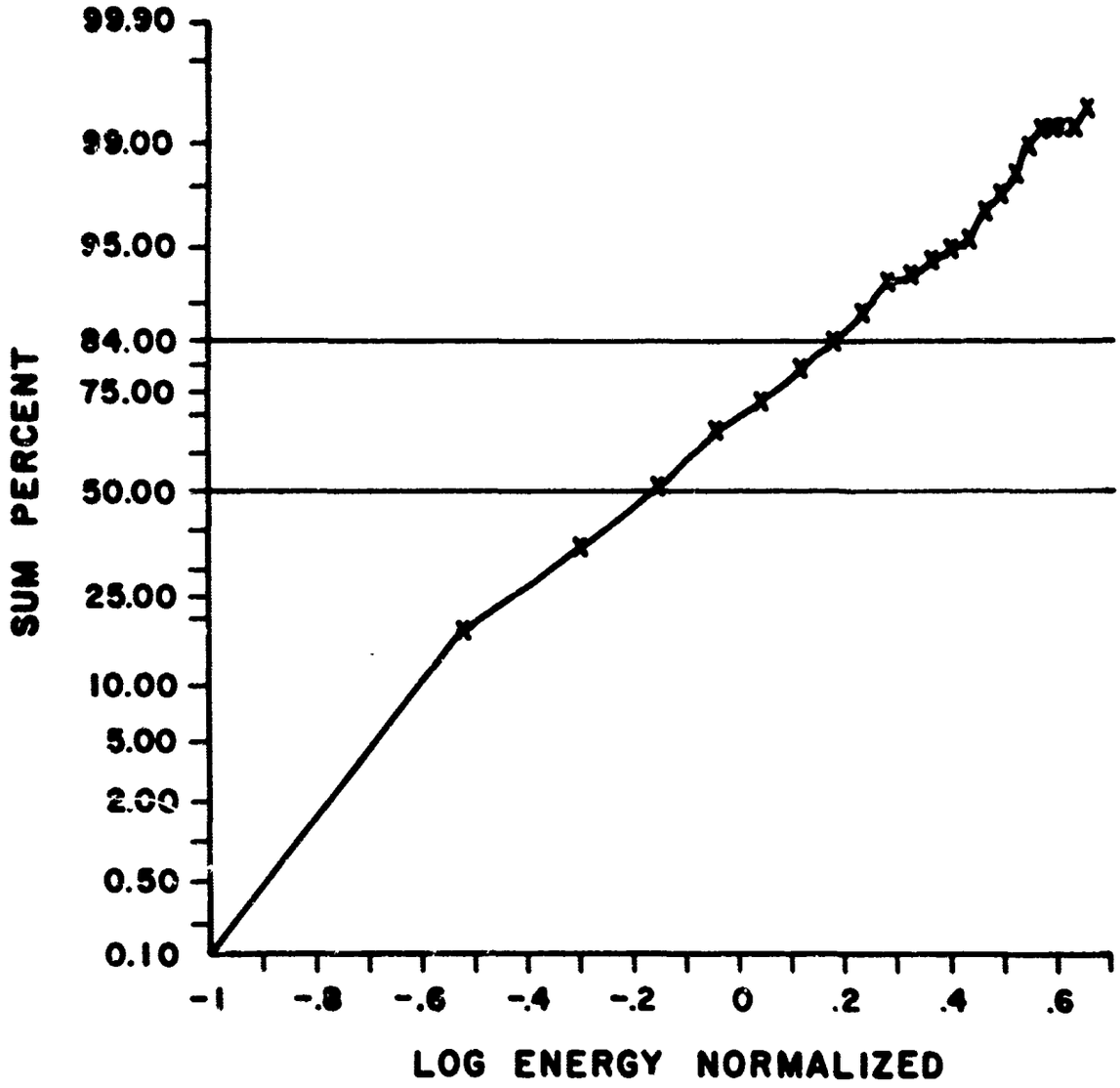

Figure 7. First cumulative distribution curve for image shown in Figure 3

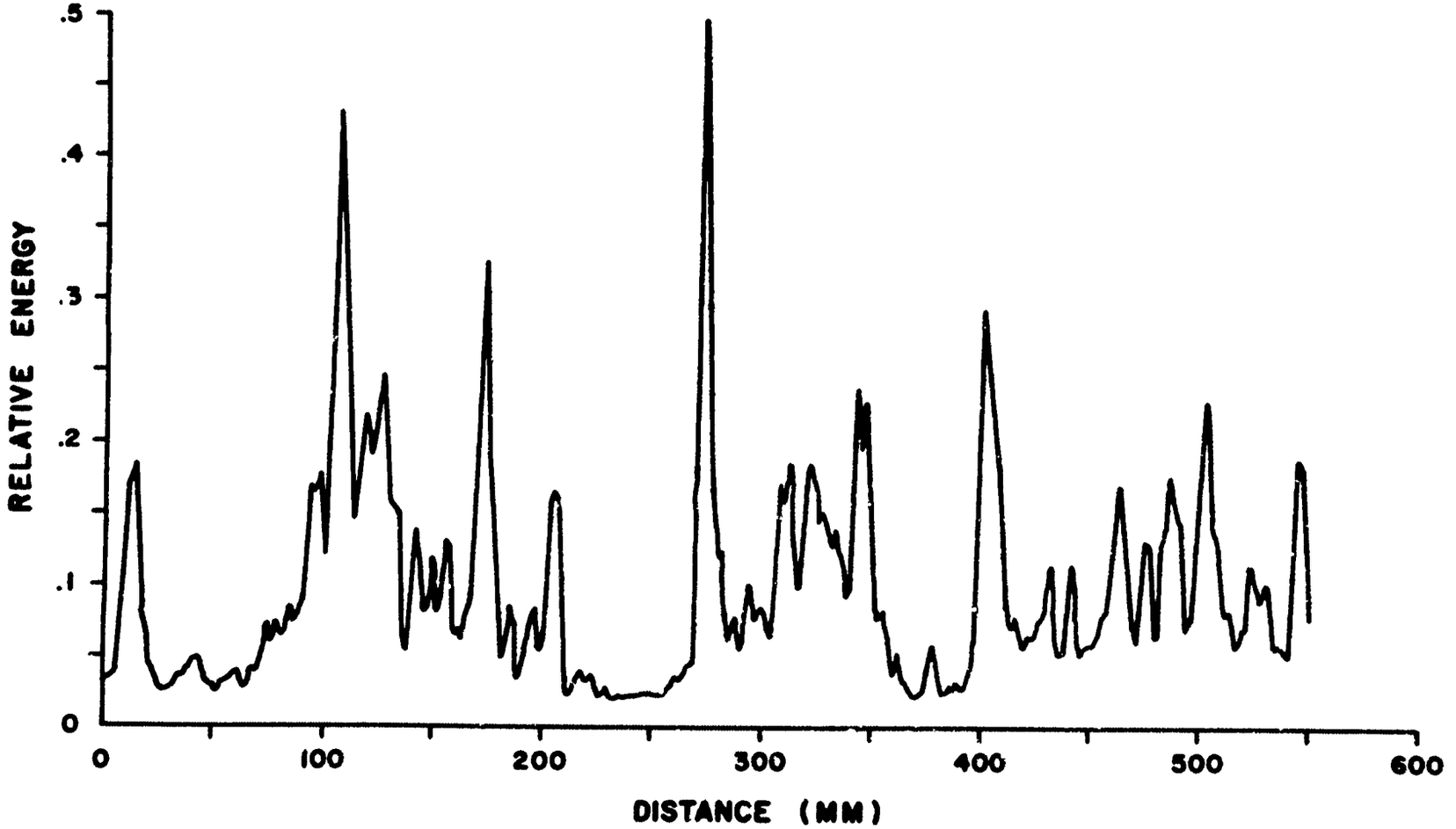

Figure 8. Second energy scan for image shown in Figure 3

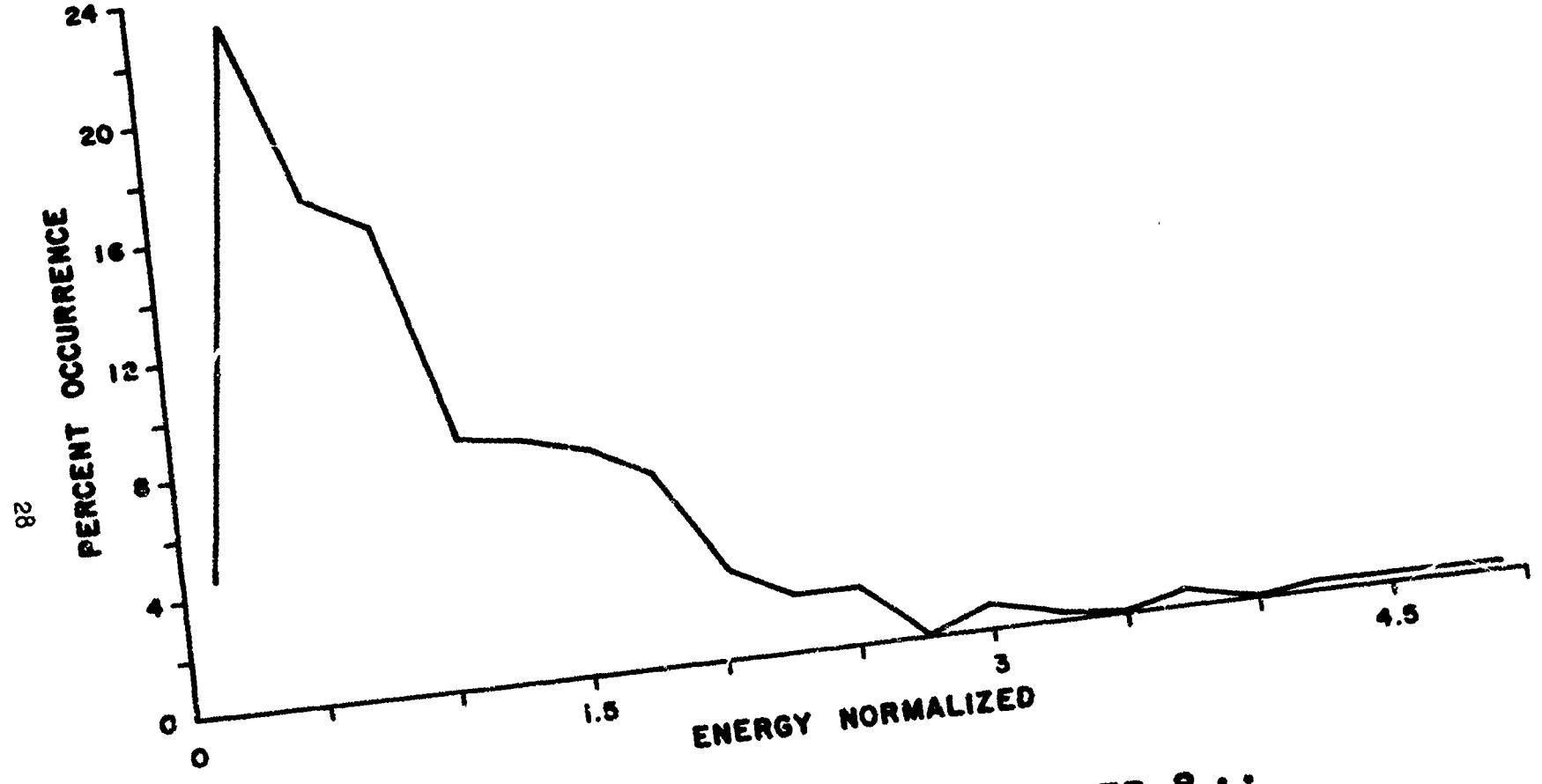

Figure 9. Second distribution curve for image shown in Figure 3

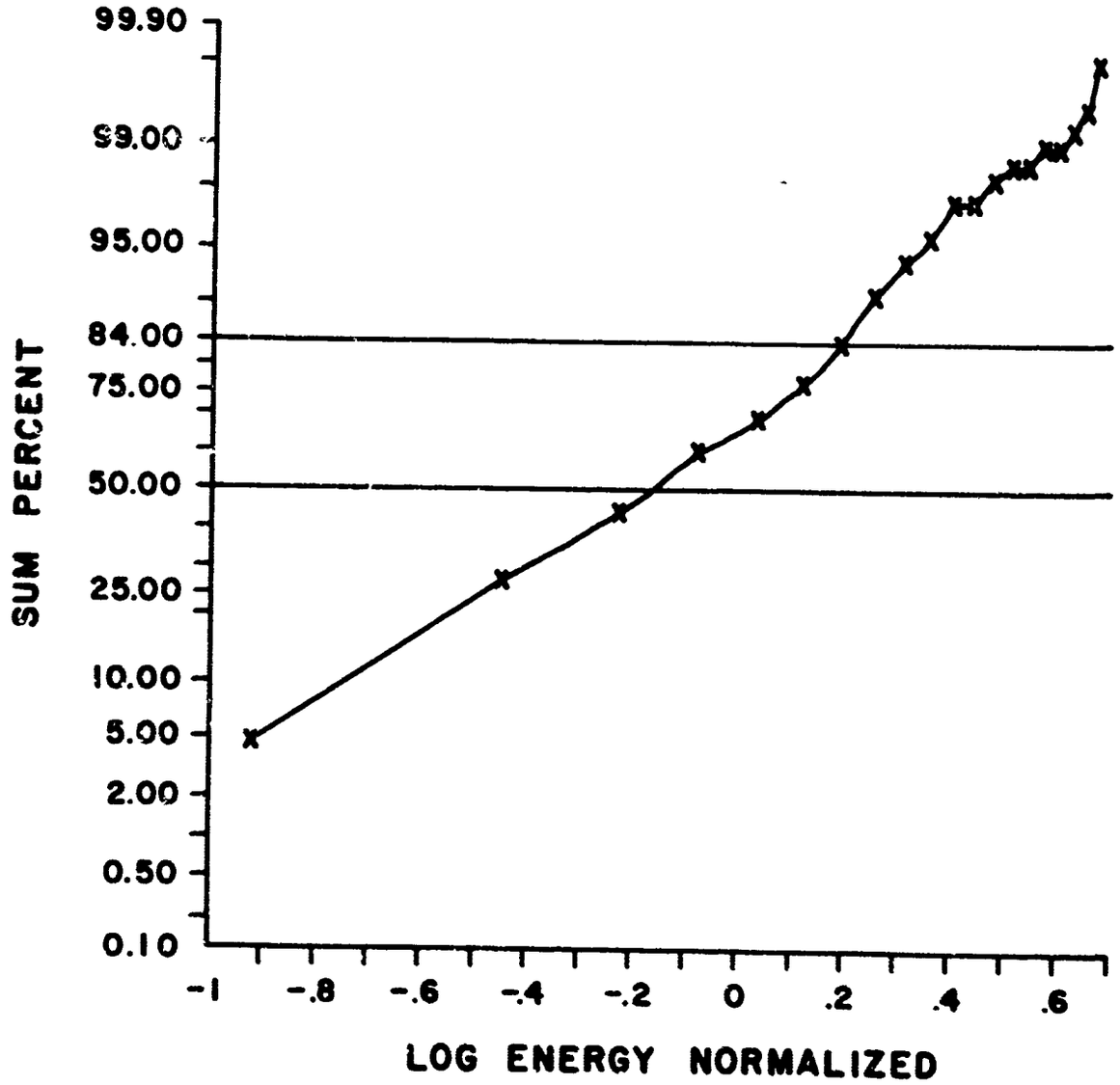

Figure 10. Second cumulative distribution curve for image shown in Figure 3

Figure 11. Cross section of laser beam at 1000 meters (Run No. 20)

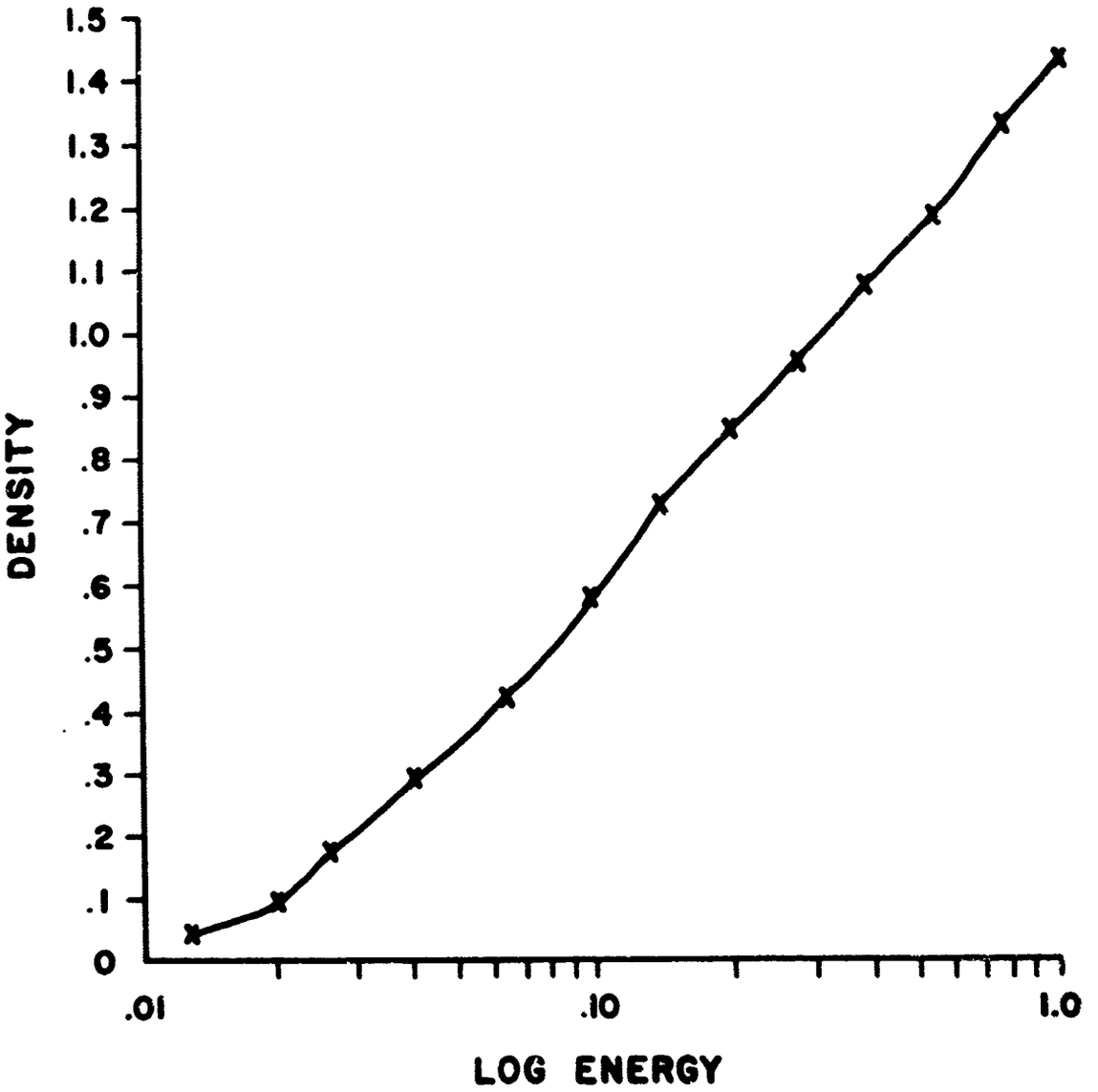

Figure 12. Characteristic curve for step wedge (Run No. 20)

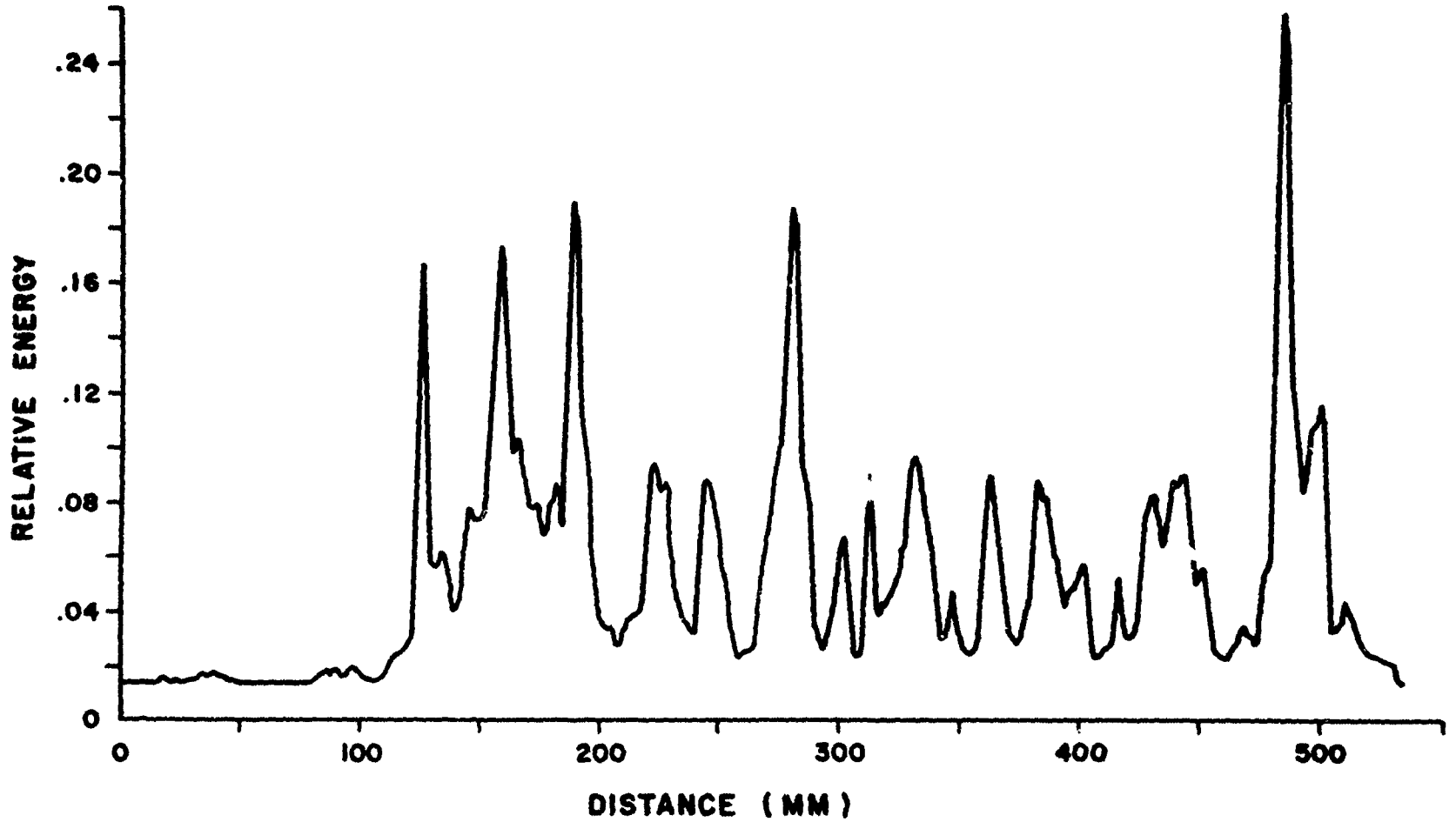

6 JUNE 67, C 14, R 1000, FR 15 .

Figure 13. First energy scan for image shown in Figure 11

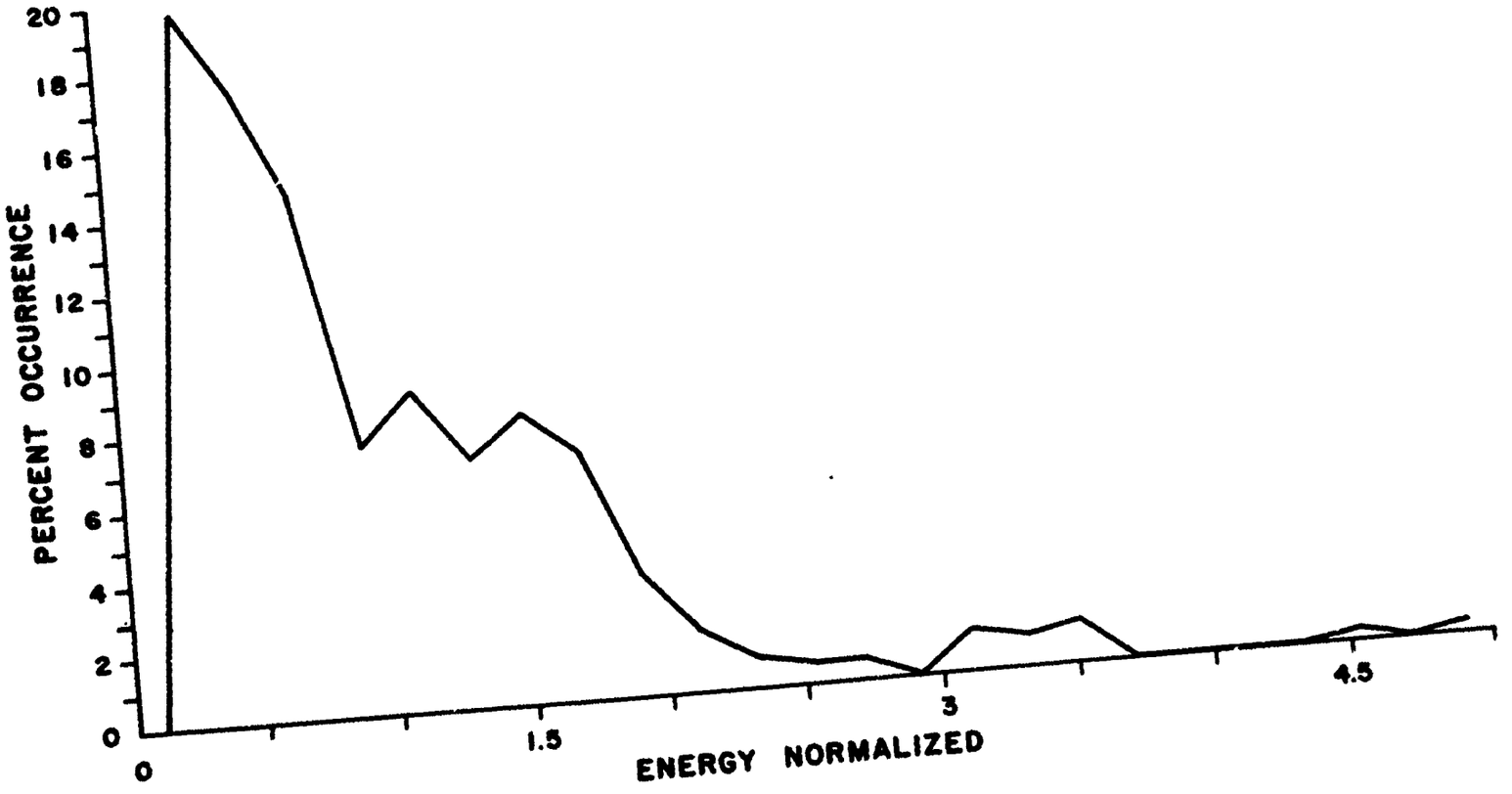

Figure 14. First distribution curve for image shown in Figure 11

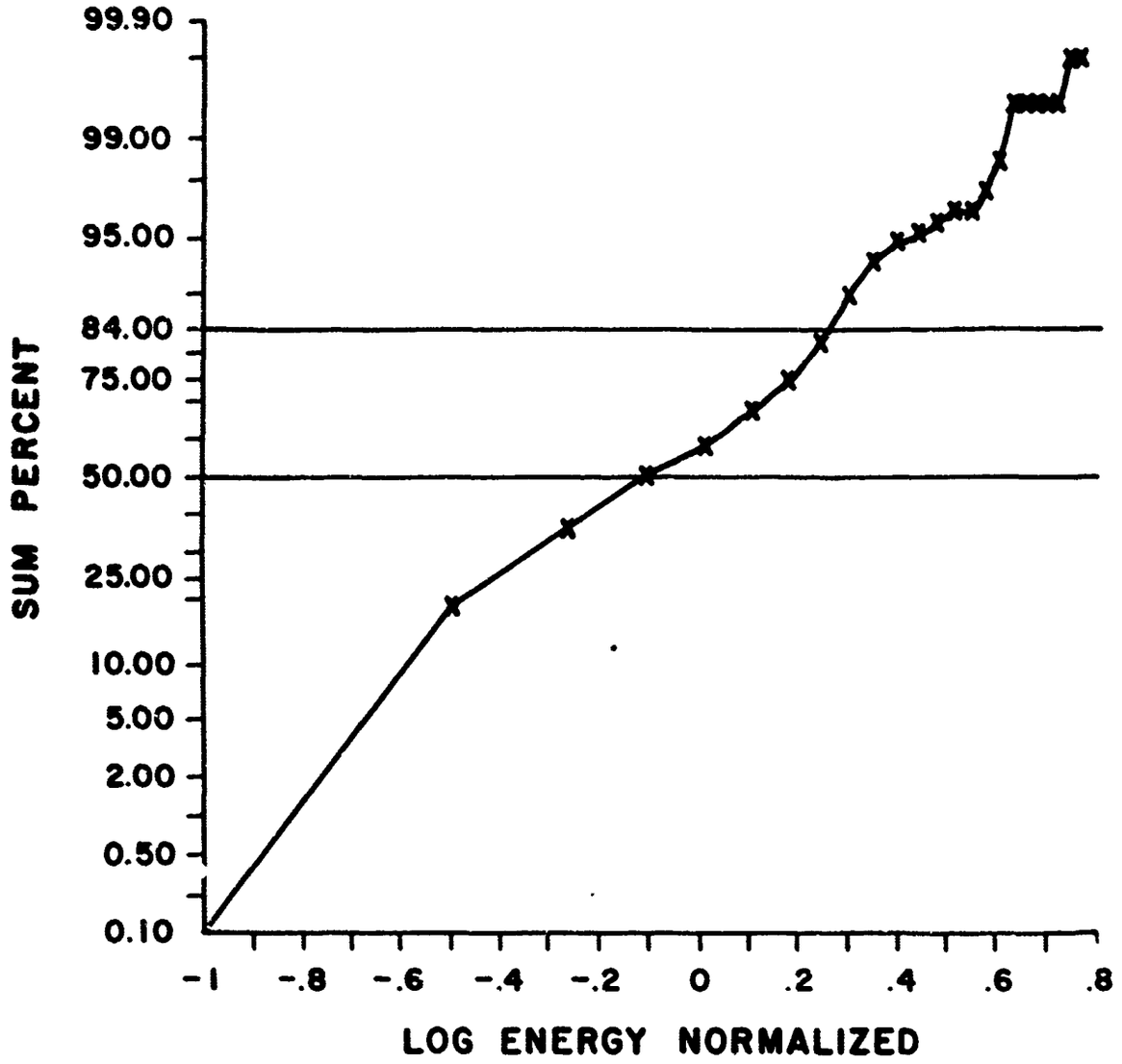

Figure 15. First cumulative distribution curve for image shown in Figure 11

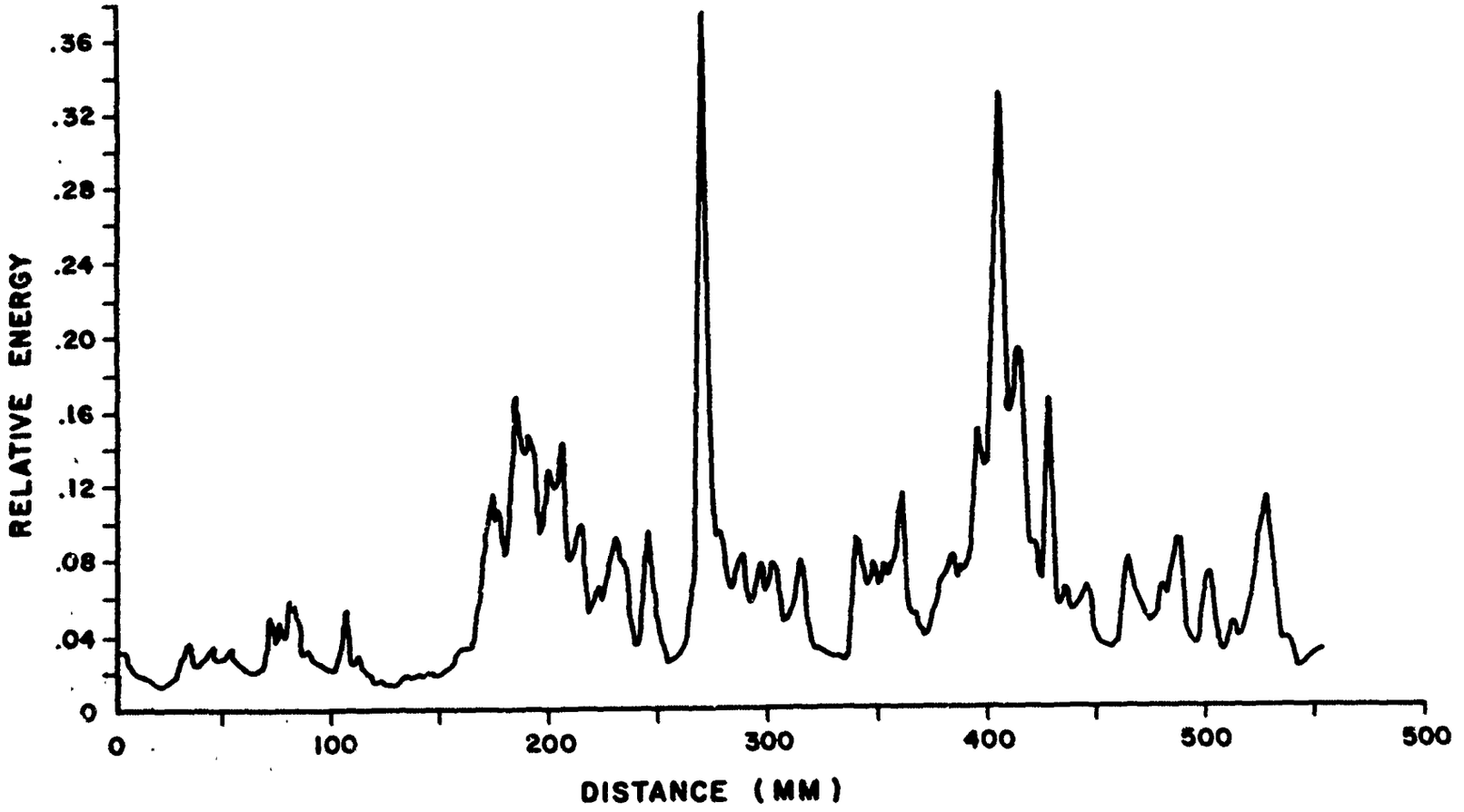

Figure 16. Second energy scan for image shown in Figure 11

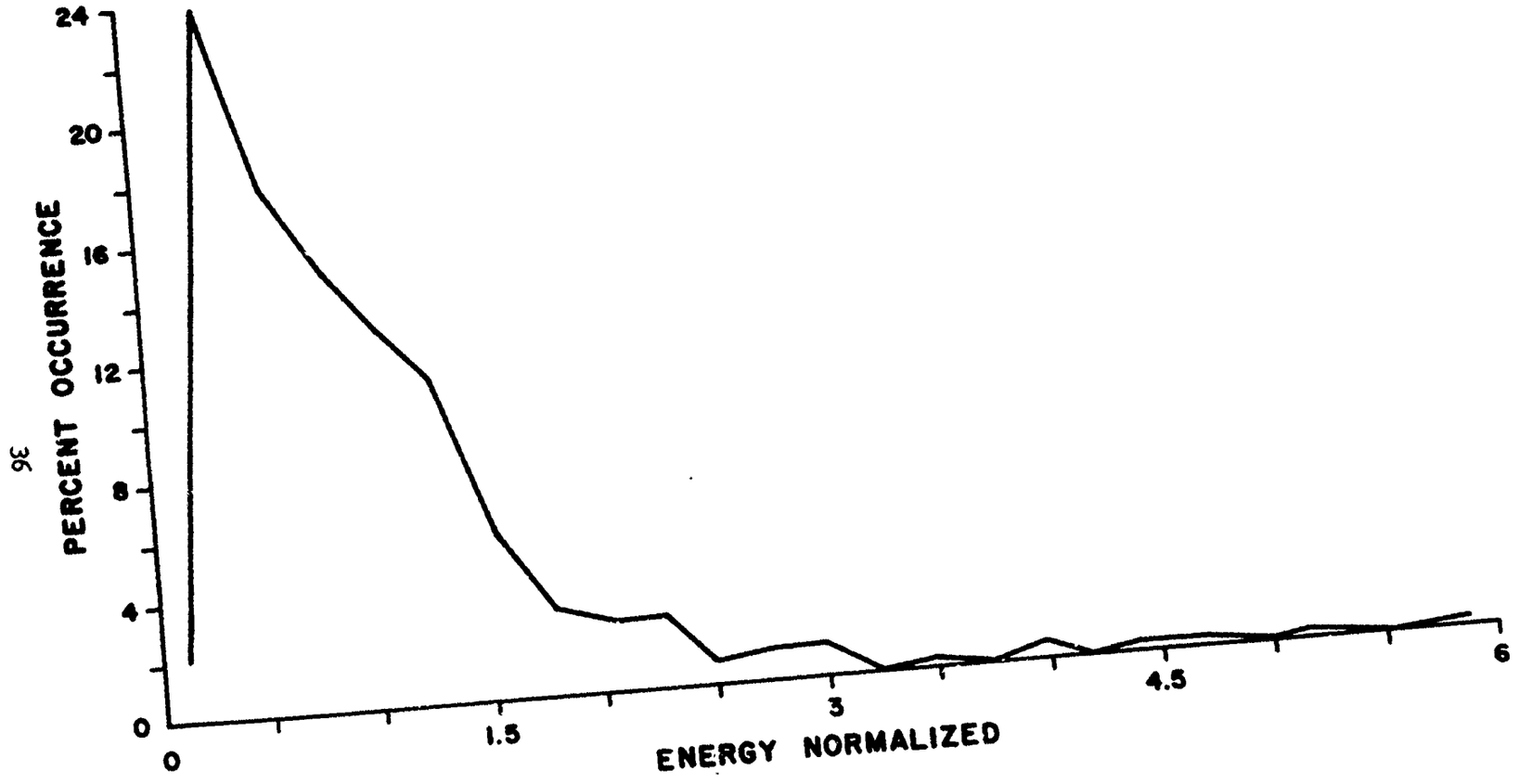

Figure 17. Second distribution curve for image shown in Figure 11

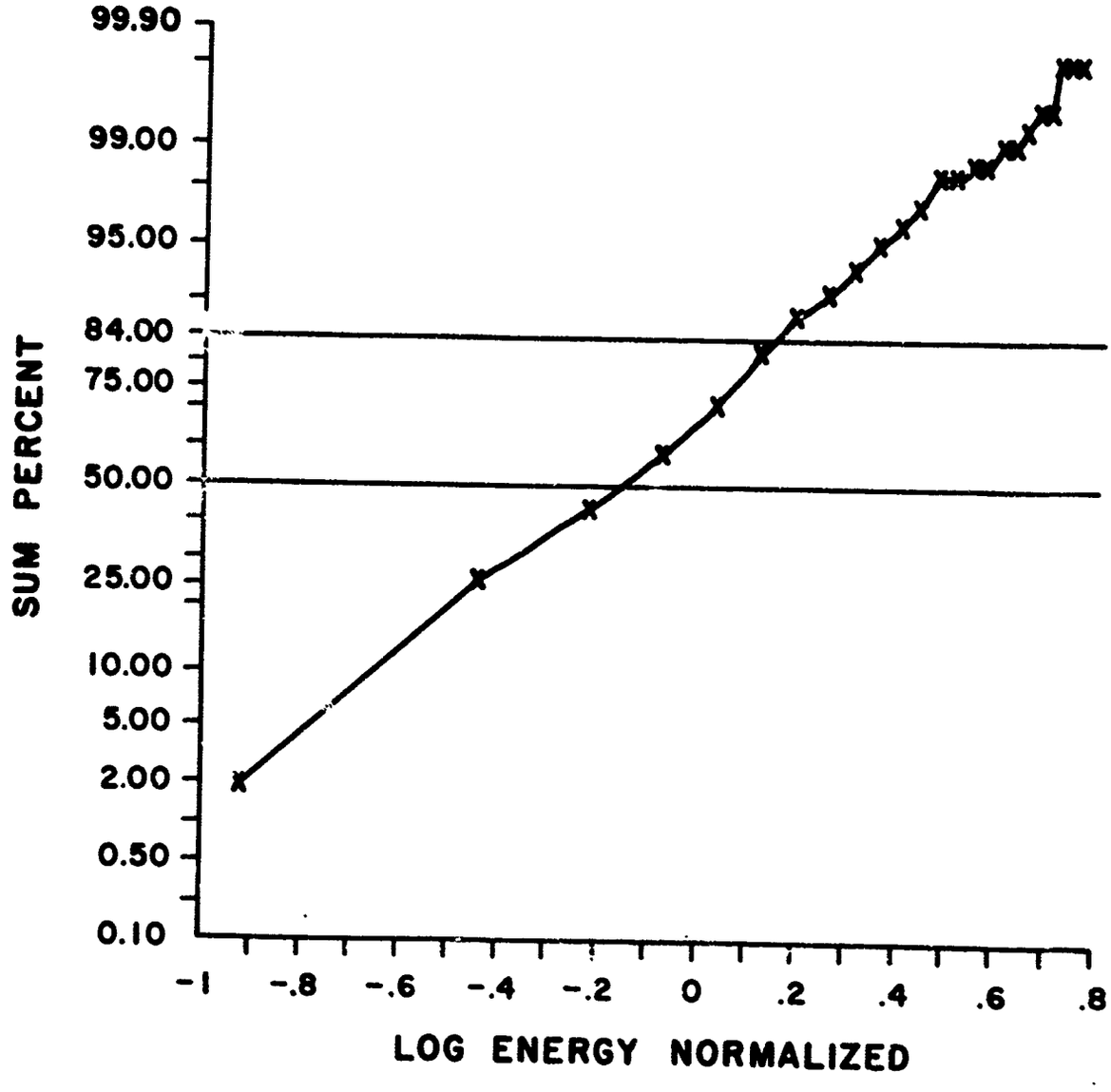

Figure 18. Second cumulative distribution curve for image shown in Figure 11

Unclassified
Security Classification

DOCUMENT CONTROL DATA - R & D

(Security classification of title, body of abstract and indexing annotation must be entered when the overall report is classified)

1. ORIGINATING ACTIVITY (Corporate author) U.S. Army Ballistic Research Laboratories Aberdeen Proving Ground, Maryland	2a. REPORT SECURITY CLASSIFICATION Unclassified 2b. GROUP

3. REPORT TITLE

ATMOSPHERIC EFFECTS ON THE BEAM PROPAGATION OF THE XM-23 LASER RANGEFINDER

4. DESCRIPTIVE NOTES (Type of report and inclusive dates)

5. AUTHOR(S) (First name, middle initial, last name)

Paul H. Deitz

6. REPORT DATE September 1967	7a. TOTAL NO. OF PAGES 53	7b. NO. OF REFS
8a. CONTRACT OR GRANT NO. b. PROJECT NO. RDT&E 1W523801A291 c. d.	9a. ORIGINATOR'S REPORT NUMBER(S) Memorandum Report No. 1871 9b. OTHER REPORT NO(S) (Any other numbers that may be assigned this report)	

10. DISTRIBUTION STATEMENT

This document has been approved for public release and sale; its distribution is unlimited.

11. SUPPLEMENTARY NOTES Presented at the "Laser Range Instrumentation Seminar-in-Depth" sponsored by SPIE held in El Paso, Texas, 16-17 Oct 67.	12. SPONSORING MILITARY ACTIVITY U.S. Army Materiel Command Washington, D.C.

13. ABSTRACT

A special optical receiver with a 2-foot input aperture was used to measure beam cross sections of the XM-23 Laser Rangefinder. The standard deviations of the received energies were determined for pathlengths from 200 to 1500 meters. The index structure constant, C_n^2, (derived from the measured thermal structure function) and the solution to the spherical wave equation were used to predict the standard deviations of the optical energy distributions. The predictions based on meterological measurements were compared to the standard deviations of the optical measurements for high scintillation conditions.

DD FORM 1 NOV 65 1473 REPLACES DD FORM 1473, 1 JAN 64, WHICH IS OBSOLETE FOR ARMY USE.

Unclassified
Security Classification

14 KEY WORDS	LINK A		LINK B		LINK C	
	ROLE	WT	ROLE	WT	ROLE	WT
Laser Rangefinder Scintillation Atmospheric Turbulence						